Macromolecules

Volume 28, Number 3 January 30, 1995

Dynamics of a 2311 Base Pair Superhelical DNA in Dilute and Semidilute Solutions

Joachim Seils† and R. Pecora*

Department of Chemistry, Stanford University, Stanford, California 94305-5080

Received March 4, 1994; Revised Manuscript Received September 14, 1994®

ABSTRACT: Dynamic light scattering–photon correlation spectroscopy (PCS) has been used to study the dynamics of a 2311 base pair (bp) superhelical plasmid DNA in dilute and semidilute solutions. In dilute solution, translational and rotational/internal modes could be resolved. Assuming that the DNA is a rigid rod, the translational diffusion coefficient determined at infinite dilution gives cylinder dimensions consistent with a calculated length L of 230 nm and a diameter of 13.4 nm. If the rotational/internal mode is interpreted as rotation of a rigid rod, the derived rotational diffusion coefficient is consistent with a shorter rod of a smaller length to diameter ratio. The dilute and semidilute regimes are clearly distinguished by a break in the concentration dependence of the mutual diffusion coefficient. The transition concentration, using the L given above, was found to lie at cL^3 between 3 and 5. In the semidilute regime, a slow mode was detected in addition to the main diffusion mode. The relative amplitude of the slow mode increases with increasing concentration until it is the dominant mode in the DLS frequency distribution. The slow mode frequency decreases with increasing concentration. The characteristics of the slow mode are not in accord with those of the slow mode predicted by the spinodal decomposition theory of Doi, Shimada, and Okano (DSO) for stiff rodlike polymers. The observed mode is consistent with the formation of aggregates in the semidilute regime. The mutual diffusion coefficient in the semidilute regime shows a linear concentration dependence, which is in qualitative agreement with the predictions of the DSO theory. The slope of this linear concentration dependence, however, differs markedly from the theoretical prediction assuming a concentration-independent self-diffusion coefficient. In addition, no deviation from quadratic scattering vector length dependence of the mutual diffusion mode, as predicted by the DSO theory, is observed. The rotational diffusion/internal relaxation frequencies appear to decrease with increasing concentration. However, the rather large scatter in the data (due to the relatively small contribution of this mode to the spectrum in the presence of the slow mode) prevented a quantitative comparison with existing theories.

I. Introduction

Much research is currently being conducted on the solution dynamics of rigid-rod macromolecules. In addition to their materials and biological importance, the strong interest in these systems arises from the fact that rigid-rod polymers are the simplest objects that exhibit entanglement in concentrated solutions. The influence of entanglements on the dynamics of polymers, both rigid and flexible, is one of the still largely unsolved problems in polymer science.[1]

The Doi–Edwards theory,[2,3] which evolved from the reptation concept for flexible molecules,[4,5] has been used with limited success to describe the dynamics (primarily the rotational relaxation) of rigid rods in semidilute solutions. Later refinements of this theory have led to better agreement with experimental observations,[6] although considerable discrepancies still remain.

Theories for the dynamics of concentrated rodlike particle solutions rely on the caging concept—the confinement of a probe rod in a cage of neighboring rods. In the original Doi–Edwards theory (DE) the cage is completely closed over an extended period of time and the infinitely thin rod can only escape by diffusion along its long axes. Within the cage, the rod performs small-angle rotations. The theory assumes a constant self-diffusion coefficient, which is half the infinitely dilute value. The theory predicts an inverse square concentration dependence of the rotational diffusion coefficient in the semidilute regime. An extension of DE by Doi, Shimada, and Okano (DSO) includes excluded-volume effects and a nematic interaction between rods.[7–9] The

† Present address: Max-Planck-Institute for Polymer Research, Ackermannweg 10, D-55128 Mainz, Germany.

® Abstract published in *Advance ACS Abstracts,* December 15, 1994.

0024-9297/95/2228-0661$09.00/0

self-diffusion coefficients are treated as adjustable parameters in this theory. Based on these assumptions, the DSO theory predicts that the cooperative diffusion coefficient that is obtained from the initial decay of the intensity autocorrelation function in a DLS experiment is scattering vector length dependent. Furthermore, the cooperative diffusion coefficient should show a linear dependence on concentration in the semidilute regime. DSO also predicts the appearance of a slow mode in the DLS autocorrelation function that should be evident near the theoretical nematic transition. The relative contribution of the slow mode should, after it becomes apparent, decrease upon further increasing the concentration. Slow modes have been observed in semidilute solutions of rodlike molecules by various authors previously.[10-12] DSO predicts the appearance of these modes in uncharged polymer solutions and gives quantitative and testable predictions of their features.

Objections to DE and related theories like DSO originate from Brownian dynamics simulation results on rodlike particles in semidilute solutions.[13-15] On the basis of such simulations, Fixman proposed an additional mechanism for the rotational relaxation of the probe rod, which for short time periods should dominate over the DE mechanism.[15] Fixman argued that simultaneous small-angle rotations of neighboring rods could allow rotational relaxation of a probe rod. In this picture, the cage also could open up more frequently and the probe rod could escape via lateral translation much more easily. In essence, in the Fixman model, the probe rod is less confined by the cage than in DE. Furthermore, the dependence of the rotational diffusion coefficient Θ on concentration c is $\Theta \sim c^{-1}$ in the Fixman formulation. This is weaker than the c^{-2} dependence of DE.

Brownian dynamics simulations by Bitsanis et al.[13,14] in moderately concentrated solutions support the Fixman model for the rotational diffusion. They also show that the transverse translational self-diffusion, although hindered by neighboring rods with increasing concentration, does not approach zero over the concentration range studied (this range is representative of that in most experimental studies). The freezing of the translational diffusion perpendicular to the long axes of the rod seems to occur at much higher concentrations in these simulations than in DE. At these higher concentrations, however, anisotropic phases are observed in experimental systems.[16,17]

Transient electric birefringence (TEB),[18-20] dynamic light scattering–photon correlation spectroscopy (PCS),[10,11,18,21-25] and holographic grating relaxation (HGR) (also called forced Rayleigh scattering) studies[12] on semidilute solutions of rodlike molecules have been used to test the predictions of the various theories. The HGR study, which monitors the self-diffusion coefficient, clearly shows that the self-diffusion coefficient of a short rodlike, double-helical DNA fragment gradually drops with increasing concentration in the semidilute regime, similar to what is seen in the Brownian dynamics simulations for hard rods. This finding indicates that one of the assumptions that is used in DE and in a version of DSO—that the self-diffusion coefficient becomes independent of concentration in the semidilute region—does not hold. This assumption is, however, not critical for the further predictions of some of the theories such as DSO, which, in the general case, treat the self-diffusion coefficients as parameters. Indeed the linear concentration dependence of the cooperative or mutual diffusion coefficient predicted by DSO, as well as the appearance of a slow mode mentioned above, were confirmed in three recent PCS studies.[11,12,21] On the other hand, although there is some evidence for the deviation from the q^2 dependence that is predicted by DSO,[10,22] the relative amplitudes of slow and fast modes do not appear to agree with the predictions of this theory. In addition, the slope of the straight line in the plot of the diffusion coefficient that is extracted from the PCS data versus concentration does not agree with the DSO prediction, if the DE assumptions about the translational self-diffusion coefficient in the semidilute region are used. Thus, DSO gives a qualitatively correct picture of some of the broad features of the experimental data but gives poor quantitative predictions on the systems studied to date.[11,21]

One uncertainty in the interpretation of experimental results is the polydispersity of the samples that are usually studied. To make the test of existing theories as stringent as possible, attempts have been made to exclude this uncertainty by performing experiments on a well-defined monodisperse homologous series. The DNAs are rather stiff molecules that can, at least as far as molecular weight is concerned, be prepared in monodisperse form. Different conformations including linear, relaxed circular, and superhelical forms of the same molecular weight can often be studied. We expect that the superhelical form of a 2311 base pair (bp) plasmid DNA would be relatively stiff and rodlike. It is also long enough so that both translational and rotational motion of the molecule can be observed by polarized PCS. This superhelical DNA and ones of comparable length have been used for PCS and TEB studies[18] in dilute solution earlier and have been regarded as rigid rods. As discussed below, our more extended results in dilute solution suggest that there are some ambiguities concerning the structure of this superhelical molecule. Nevertheless, even though it might have some shape irregularities or flexibility, this DNA is relatively elongated and stiff and constitutes an excellent model system for studying entanglements in nondilute solutions. It is also, of course, of interest as a representative of an important class of biological macromolecules.

II. Theories of Rod Dynamics

2.1. Rigid Rods at Infinite Dilution. Neglecting rotational–translational coupling, the molecular dynamic structure factor $S(q,t)$ can be written as[26]

$$S(q,t) = S_0(qL)\exp(-q^2D_0t) + S_1(qL)\exp[(-(q^2D_0 + 6\Theta_\perp)t] + \ldots \quad (1)$$

with D_0 the translational self-diffusion coefficient

$$D_0 = \frac{1}{3}(D_\parallel + 2D_\perp) \quad (2)$$

and $\Theta_\perp$ the rotational self-diffusion coefficient around an axis which is perpendicular to the long axis of the rod.[27] The weights S_0 and S_1 are functions of the product of the scattering vector length q and the rod length L. They have been calculated by Pecora.[27] Basically, at low qL all of the intensity is in the first term. The time decay of this term depends only on the translational diffusion coefficient, while at higher qL the second exponential also becomes important, allowing

extraction of the rotational diffusion coefficient from the data. Corrections to eq 1 due to translational–rotational coupling of long rods have been computed by several authors.[28–30] They lead to lower amplitudes in the faster mode and faster apparent rotational relaxation times. The translational diffusion also appears to speed up. In order to obtain an appreciable contribution of translational–rotational coupling in dilute solution, however, the axial ratio of the rod must be high. In such a case $D_\perp$ and $D_\parallel$ are very different and the coupling is strong. In semidilute solution the coupling is likely to become stronger since $D_\perp$ could be severely decreased due to interrod interactions.

For rigid molecules the diffusion coefficients in eq 1 can be calculated from hydrodynamic theories. For ellipsoids of revolution, for instance, this has been done by Perrin.[31] For cylinders or rods, however, the functions show singularities at the ends of the cylinder. In the approach of Tirado and Garcia de la Torre this difficulty is circumvented by replacing the rod by stacks of rings constructed from a number of beads.[32,33] Using a rigorous version of the Kirkwood–Riseman theory,[34] Garcia de la Torre et al. give a method for calculating the transport coefficients of any assembly of beads by solving eq 3 for the frictional force $\mathbf{F}_i$ of bead i.[35,36]

$$\mathbf{F}_i = \xi \sum_{j=1}^{N} \mathbf{S}_{ij} \cdot (\mathbf{u}_j - \mathbf{v}_j^\circ) \tag{3}$$

where ξ is the frictional coefficient of a bead and $\mathbf{u}_j$ and $\mathbf{v}_j^\circ$ are respectively the velocity of bead j and the unperturbed velocity of the solvent at the center of this bead. The $\mathbf{S}_{ij}$s are the 3×3 blocks of the inverse of a $3N \times 3N$ super matrix $\mathbf{Q}$ ($\mathbf{S} = \mathbf{Q}^{-1}$) which depends only on the coordinates $\mathbf{R}$ of the N beads through eq 4.

$$\mathbf{Q}_{ij} = \delta_{ij}\mathbf{I} + (1 - \delta_{ij})\xi\,\mathbf{T}_{ij} \tag{4}$$

Here δ_{ij} and $\mathbf{I}$ are the Kronecker delta and the three-dimensional unit tensor, respectively. The $\mathbf{T}_{ij}$s are the elements of the modified hydrodynamic interaction tensor formulated by Rotne and Prager,[37] and Yamakawa[38] that is defined by

$$\mathbf{T}_{ij} = \frac{1}{8\pi\eta R_{ij}}\left[\mathbf{I} + \frac{\mathbf{R}_{ij}\mathbf{R}_{ij}}{R_{ij}^2} + \frac{b^2}{2R_{ij}^2}\left(\frac{1}{3}\mathbf{I} - \frac{\mathbf{R}_{ij}\mathbf{R}_{ij}}{R_{ij}^2}\right)\right] \tag{5}$$

where b is the bead diameter and η the solvent viscosity. Equation 5 is valid for nonoverlapping beads $R_{ij} > b$. The hydrodynamic properties of the object are defined by the translational Ξ_t, coupling $\Xi_{O,c}$, and rotational $\Xi_{O,r}$ friction tensors given by

$$\Xi_t = \xi \sum_{i=1}^{N}\sum_{j=1}^{N} \mathbf{S}_{ij} \tag{6}$$

$$\Xi_{O,c} = \xi \sum_{i=1}^{N}\sum_{j=1}^{N} \mathbf{R}_i \times \mathbf{S}_{ij} \tag{7}$$

$$\Xi_{O,r} = \xi \sum_{i=1}^{N}\sum_{j=1}^{N} \mathbf{R}_i \times \mathbf{S}_{ij} \times \mathbf{R}_j \tag{8}$$

In the rigid-body approximation, these quantities can be obtained solely from the coordinates of the beads by inversion of the super matrix $\mathbf{Q}$. In eqs 7 and 8 the cross $\times$ denotes a dyadic product, and the coupling and rotational friction tensors depend on the origin of the center of coordinates as indicated by the index O. From eqs 6–8, the transport coefficients can be calculated using the bead subunit model from eqs 11–18 of ref 35.

From the special case of rigid rods, simple expressions for the diffusion coefficients may be obtained by extrapolating the results of bead size $\to 0$ and letting the number of beads $\to \infty$. It is found that $D_\perp$, $D_\parallel$, and $\Theta_\perp$ can be expressed as functions of the axial ratio $\varrho = L/d$, where L is the length and d the diameter of the rod.

$$D_\perp = \frac{k_B T}{4\pi\eta L}(\ln(\varrho) + \nu_\perp) \tag{9}$$

$$D_\parallel = \frac{k_B T}{2\pi\eta L}(\ln(\varrho) + \nu_\parallel) \tag{10}$$

$$\Theta_\perp = \frac{3k_B T}{\pi\eta L^3}(\ln(\varrho) + \delta_\perp) \tag{11}$$

In eqs 9–11, k_B is the Boltzmann constant, T is the absolute temperature, and $\nu_\perp$, $\nu_\parallel$, and $\delta_\perp$ are "end-effect corrections", which can be expressed as polynomials in ϱ as follows:

$$\nu_\perp = 0.839 + 0.185/\varrho + 0.233/\varrho^2 \tag{12}$$

$$\nu_\parallel = -0.207 + 0.980/\varrho - 0.133/\varrho^2 \tag{13}$$

$$\delta_\perp = -0.662 + 0.917/\varrho - 0.050/\varrho^2 \tag{14}$$

Equations 9–14 have been used with great success by Eimer et al. to determine the axial ratio of rodlike oligonucleotides in solution from rotational and translational diffusion coefficients.[39] In particular, it was shown that a single diameter, which is the same as the one determined by X-ray scattering methods on DNA fibers, is sufficient to reproduce the dynamics of a series of oligonucleotides. The approach summarized in eqs 3–8 is used in section 4.3 to compute translational and rotational diffusion coefficients for irregular shapes.

2.2. Virial Regime for Rods. Equations 9–14 give expressions for the translational and rotational self-diffusion coefficients of a rigid rod at infinite dilution. Light scattering usually measures the mutual diffusion coefficients, which are equal to the self-diffusion coefficients, in general, only at infinite dilution. Because of the difficulties of treating the many-body problems involved in their computation, a macroscopic point of view starting with the phenomenological transport equation is usually adopted. In this picture, the mutual (translational) diffusion coefficient D_m is expressed in terms of frictional and thermodynamic contributions[26,40,41]

$$D_m = (M/N_A f(c_w))(1 - \nu_s)(\partial\Pi/\partial c_w)_T \tag{15}$$

with M the molecular weight, N_A Avogadro's number, c_w the polymer weight concentration, and ν_s the specific volume of the polymer. The function $f(c_w)$ is the concentration-dependent friction coefficient and $(\partial\Pi/\partial c_w)_T$ the concentration derivative of the osmotic pressure. The friction coefficient that appears here is the same as that for sedimentation. It is, except at infinte dilution, not generally equal to that for self-diffusion. Virial expansion of the osmotic pressure and power series expansion in the concentration of the friction coefficient connects the mutual diffusion coefficient to the infinite-dilution self-diffusion coefficient D_0 accord-

ing to eq 16

$$D_m = D_0(1 + k_D c_w + ...) \quad (16)$$

and

$$k_D = 2MA_2 - \nu_s - k_f \quad (17)$$

A_2 is the osmotic second virial coefficient, which can be calculated for uncharged hard rigid rods and experimentally determined by total intensity light scattering. Ishihara derived the most general form for A_2 for hard rods[41]

$$A_2 = (\pi N_A d^2 L/M^2)s \quad (18)$$

where

$$s = \frac{1}{4}\varrho\left[1 + \frac{3+\pi}{2\varrho} + \frac{\pi}{4\varrho^2}\right] \quad (19)$$

The diameter d of the rod in this case is strictly a geometric diameter, which might be different from the hydrodynamic diameter. However, Eimer et al.[39] indicate that they are likely to be the same for DNA.

For the linear coefficient in the concentration expansion of the friction coefficient, k_f, Peterson[42] has derived the expression

$$k_f = \frac{N_A k_B T}{3\eta}\frac{L^2}{D_0 M}\left(\frac{3d}{8L}\right)^{2/3} \quad (20)$$

A modifed form of the Peterson expression has been given by Itou et al.[43] These expressions give similar predictions for k_f and are in agreement with measurements on PBLG in dimethylformamide by Tracy and Pecora.[24] For charged systems like DNA in water-based buffers, however, available experimental results indicate poor agreement.[11] From eqs 15–20, the concentration dependence of the mutual diffusion coefficient in the virial regime for uncharged rigid rods can be calculated from the infinite-dilution self-diffusion coefficient. In the semidilute regime, where the rods are highly entangled, new concepts are required to describe the rod diffusion.

2.3. Rigid Rods in the Semidilute Regime. Theories for the rotation and translation of rodlike particles in the semidilute regime have been briefly reviewed in the Introduction. We present here some of the main quantitative results that are used in our analyses in sections IV and V.

The Doi–Edwards theory postulates a microscopic mechanism for self-diffusion and then derives the resulting consequences for observable properties like the dynamic structure factor. In the original DE, complications due to interactions among the rods other than entanglement are ignored. According to the DE postulates, perpendicular translational diffusion (see eq 9) is completely frozen, while parallel diffusion is unaffected by concentration increases and remains at its infinite-dilution value (eq 10). Due to caging from neighboring rods, the rotational diffusion coefficient Θ_m of the long axis of a rod in the semidilute region is related to that at infinite dilution by

$$\Theta_m = \beta\Theta_\perp/c^2L^6 \quad (21)$$

where β is a prefactor of order 1–10 and c the number density. This result should be compared with the weaker c^{-1} dependence in the Fixman[15] model described in the Introduction.

The DSO[7-9] approach relies on the same picture as DE. However, the self-diffusion coefficients are generally regarded as adjustable parameters. Interactions other than entanglement are accounted for by a nematic interaction potential. The theory predicts an isotropic to nematic phase transition. In the isotropic phase, the cooperative diffusion coefficient D_{coop}, defined by the first cumulant Γ_c of the dynamic structure factor, is found to be

$$D_{coop} = \Gamma_c/q^2 = (1 + 8c/c^*)D_G[1 + B(c)\,(qL)^2] \quad (22)$$

and

$$D_G = \frac{1}{3}(D_\parallel^a + 2D_\perp^a) \quad (23)$$

$$B(c) = \frac{1}{36}\left(\frac{1}{10} - \frac{8c}{c^* + 8c}\right) \quad \text{in dilute solution} \quad (24)$$

$$B(c) = -\frac{1}{9}\left(\frac{1}{5} + \frac{2c}{c^* + 8c}\right) \quad \text{in concentrated solution} \quad (25)$$

$$c^* = 16/\pi dL^2 = 4/A_2 \quad (26)$$

The self-diffusion coefficients in eq 23 have been indexed to indicate that they are adjustable parameters. They are, in general, concentration dependent and therefore are likely to differ from the ones calculated from eqs 9 and 10. The most pertinent results of DSO to our work are the linear concentration dependence of D_{coop} in the $q \to 0$ limit and its q^2 dependence in the semidilute region. In the work of Goinga and Pecora,[11] D_{coop} has been identified with D_m from eq 16.

Close to the spinodal decomposition, the DSO theory predicts the appearance of a slow mode. The relaxation frequency Γ_s of this mode is given by

$$\Gamma_s = \frac{D_\parallel^a q^2(c^* + 8c)(15 + 4\alpha)}{45c^*} \quad (27)$$

The ratio of the amplitudes of the Γ_s mode to the Γ_c mode is

$$A_s/A_c = \beta/\alpha \quad (28)$$

α and β ($\alpha < \beta$) are the solutions of the following quadratic equation:

$$28(8c + c^*)x^2 - 15(4c^* - 67c)x - 315(c^* - c) = 0 \quad (29)$$

2.4. Modeling Superhelical DNA as a Rigid Rod. Since typical scattering vector lengths in light scattering experiments are on the order of several nanometers, the local superhelical structure of the plasmid DNA will not be directly observed and we can model the DNA as a more smooth structure. We assume that the DNA forms a resultant structure that may be approximated by a rigid cylinder of length L and diameter d. In order to calculate the dimensions of an equivalent rigid cylinder for superhelical DNA, we start with the general helix equation[44] which expresses the length of one helical turn as a function of diameter and pitch,

$$L_H^2 = 4\pi^2 r^2 + p^2 \quad (30)$$

where L_H is the length of one helical turn, r the radius, and p the pitch of the helix. If we substitute r by the pitch angle a_p with

$$\tan(a_p) = r/a \quad (31)$$

and

$$p = 2\pi a \quad (32)$$

we obtain for the pitch to helix length ratio

$$p/L_H = \left(\frac{1}{1 + \tan^2(a_p)}\right)^{1/2} \quad (33)$$

Identifying the contour length of the cylinder that is equivalent to the superhelical DNA with $n_\theta p$ and the total helix length $= n_\theta L_H$ with half the contour length of the circular DNA, L_l, we have

$$n_\theta L_H = L_l/2 = (n_b - 1)l/2 \quad (34)$$

where n_θ is the number of helical turns in the molecule, n_b the number of base pairs, and l the average distance between base pairs. The rod length can be calculated from n_b, l, and a_p, which are known for our particular DNA.

In order to calculate the diameter d of the equivalent rod, one has to recognize that

$$d = 4r + d_0 \quad (35)$$

where d_0 represents the diameter of the relaxed DNA. Substitution of eqs 31–35 into the helix equation (30) leads to

$$d = (n_b - 1)\frac{l \sin(a_p)}{n_\theta \pi} + d_0 \quad (36)$$

To solve eq 36 for d, the number of (super)helical turns, n_θ, for the DNA must be known. This can be obtained from the superhelix density—the number of superhelical turns per base pair, δ_b, of the molecule. This quantity is known for DNA from unwinding experiments of superhelical DNA by intercalation of ethidium bromide.[45] The number of superhelical turns is then given by

$$n_\theta = \delta_b n_b / n_h \quad (37)$$

where n_h is the number of base pairs for one turn. Substituting $a_p = 55°$,[46] $d_0 = 2$ nm, $n_b = 2311$, $l = 0.346$ nm, $\delta_b = 0.079$,[47] and $n_h = 10$ into eqs 33, 36, and 37, we obtain the equivalent rod dimensions: length $L =$ 230 nm and diameter $d = 13.4$ nm. If a smaller pitch angle (45°) is assumed, then $L = 283$ nm and $d = 12$ nm. In the following, we use the results derived with the larger pitch angle, which appear to be in somewhat better agreement with experiment.

III. Materials and Methods

3.1. Sample Preparation. The 2311 bp superhelical plasmid DNA was prepared in our laboratory with a modified procedure of one that was described elsewhere.[48] The second alkaline precipitation was performed with a 7.5 M ammonium acetate solution (pH 7.5).[49] The precipitation on and elution from glass powder was replaced by DNAse-free RNAse treatment followed by a double (or step gradient) density dye centrifugation.[50] From a 2-L culture, 300 μg of 2311 bp DNA was obtained. The plasmid was checked for impurities with gel electrophoresis on a 1% agarose gel. In all cases a single band was observed on these gels. For the dynamic light scattering experiments the plasmid was dissolved in TE buffer containing 0.15 M sodium chloride. The solution was dialyzed against the same buffer and then centrifuged at 20 000 rpm to remove dust. The upper part of the solution was then transferred to a carefully cleaned and dust-free scattering cell. All samples were determined to be "dust free" by observation of the laser beam in the sample with a 5× magnification microscope, as described previously.[50] After the solution was directly poured into the scattering cell, it was again centrifuged at 4000 rpm. Different concentrations were prepared by diluting the sample with buffer directly in the scattering cell. When the cell was almost full and a slow mode could not be detected (see below), a small amount of the sample was filtered through 0.45-μm Millipore filters into a second carefully cleaned and dust-free scattering cell. Subsequent dilutions were carried out in this cell. This procedure was used because of the small amounts of sample available and the fact that the most concentrated samples (above about 1 mg mL^{-1}) did not pass through 0.45-μm filters. It should be emphasized, however, that the slow mode (see below) disappeared upon dilution *before* filtration. The concentrations were determined by weighing the samples before and after dilution and by measuring the UV absorption of the last concentration. When the sample did not pass the dust check after dilution, it was refiltered. Gel electrophoresis was repeated several times during the PCS measurements to check for degradation of the plasmid. No degradation products were observed over the time period of the light scattering experiments (approximately 1 month).

3.2. Photon Correlation Experiment and Data Treatment. The correlation functions were measured with a BI2030 correlator from Brookhaven instruments with linear time channels. For higher concentrations the limited time range was not sufficient to measure the whole decay of the function. Therefore, several measurements with different time increments were taken and spliced. The time increment for the first measurement was chosen in such a way that measured and calculated base lines agreed within 0.1%. The next correlation function was then taken with a factor of 4 smaller time increment. The procedure guaranteed an overlap of $N_0 = NC/4$ points. NC is the number of channels of the correlator, which was 128. As long as the time increments were above 1 μs another correlation function was measured. In most cases up to four correlation functions were spliced.

As mentioned above, up to four correlation functions were spliced. The data were not normalized prior to splicing. For the normalization the calculated base line of the correlation function with the largest sample time increment was used. Starting with the correlation function with the smallest sample time, the time overlap of this function with the one which had the factor of 4 larger sample time was determined. The first function was extrapolated for the times determined by the time of the channels of the next function by a cubic spline in the overlap region. Using the method of least squares, a two-parameter fit with the extrapolated values of the correlation function $y_1(t_2(i))$ was performed according to

$$\sum_{i=1}^{N_0} (y_2(t_2(i)) - a y_1(t_2(i)) + b)^2 = \text{minimum}$$

$y_2(t_2(i))$ represents the correlation function at the time of the second correlation function $t_2(i)$ of channel i in the overlap region. a and b are the parameters to be determined. Finally the new points $y_n(i)$ of the first correlation function which are not in the overlap region are calculated from the old ones $y_0(i)$ according to

$$y_n(i) = a y_0(i) + b$$

The points of the first correlation function are discarded

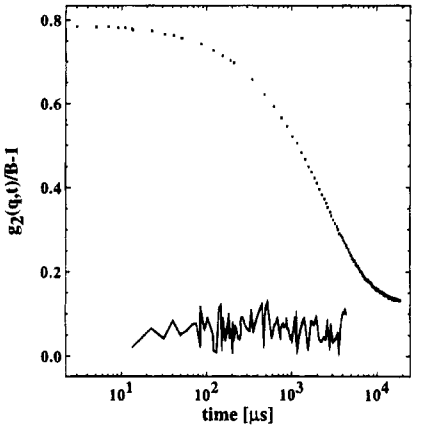

Figure 1. Spliced, normalized second-order autocorrelation function ($g_2(q,t)$) for the 2311 bp superhelical DNA. B represents the calculated base line. The scattering angle was 57° and the concentration 3.8 mg mL^{-1} at a temperature of 20 °C. The figure shows four separately measured correlation functions with sample times of 2, 8, 34, and 137 μs that have been spliced. The residuals, which are shown in the lower part of the figure, are calculated from the extrapolated value for $g_2(q,t)$ of function i and the actual values of function $i + 1$. They are therefore only defined in the time overlap region between two functions. See the text for more details about the splicing procedure.

starting at the second point of the following function. The points of the second correlation function starting from the second point to the end are appended to the $y_n(i)$ of the first function. The next cycle starts with this new function as the first function appending the next with larger sample time in the same way as before (see Figure 1).

The spliced correlation functions were finally analyzed by CONTIN to obtain a frequency distribution. The chosen solution according to the original criterion by Provencher was used.[51,52] CONTIN was first run with frequency limits given by the first and last points (base-line channels excluded) of the correlation function. The frequency distribution was calculated for 40 grid points. When the distribution was zero at more than one grid point at the ends, the frequency limits were narrowed and a second Laplace inversion was performed.

IV. Results

4.1. Correlation Functions and Frequency Distributions. A typical normalized, spliced intensity autocorrelation function for superhelical DNA is displayed in Figure 1. For the highest concentration measured (3.8 mg mL^{-1}, $cL^3 = 33.3$) the decay spans a time range of 5 orders. The splicing, as judged by the residuals in the overlap region of the different spliced functions and the fact that there were no discontinuities between different segments of the correlation function, appeared to be successful.

For different concentrations, frequency distributions as a function of scattering angle were obtained using CONTIN. The concentration dependences of the frequency distributions at two different scattering angles are shown in Figures 2 and 3. The general features of the distributions are the same for both scattering angles. In dilute solutions, ranging up to 1 mg mL^{-1} we observe essentially two processes. The main peak can be attributed to the translational diffusion of the molecule since it is proportional to q^2. A smaller peak which increases in importance with increasing scattering vector length is due to rotational and/or internal motions of the molecule. For concentrations higher than 1 mg mL^{-1}, we observe an additional slow mode in the frequency distributions. The contribution of the slow mode to the total relaxation increases with increasing

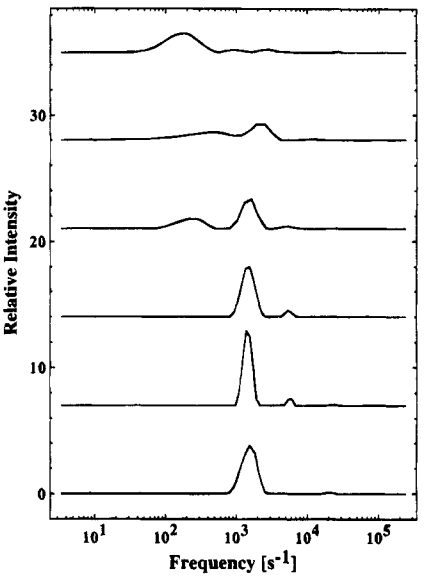

Figure 2. Frequency distributions as functions of concentration. The concentrations from top to bottom are 3.8, 2.6, 1.6, 1.1, 0.20, and 0.06 mg mL^{-1}. The corresponding correlation functions have been collected at a scattering angle of 57° and a temperature of 20 °C.

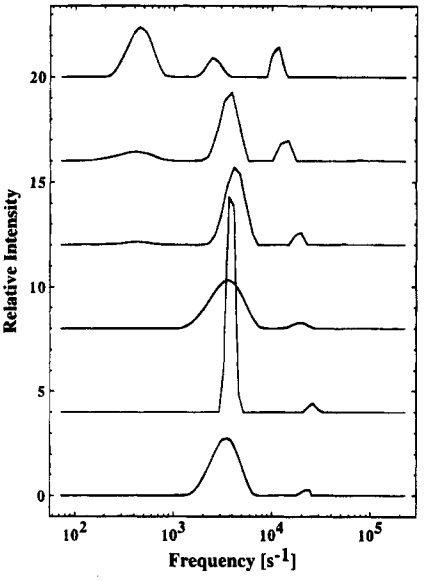

Figure 3. Frequency distributions at a scattering angle of 90° as functions of concentration. The concentrations and the temperature are the same as those in Figure 2.

concentration as clearly seen in Figures 2 and 3. The different modes are well separated in most of the frequency distributions obtained.

4.2. Translational and Rotational Dynamics in the Dilute Regime. The dimensions of the plasmid DNA in dilute solution can be determined from the rotational and translational relaxation times obtained from the DLS frequency distributions. Taking the two lowest concentrations and averaging over different angles, we obtain the values for the translational diffusion coefficient and the rotational relaxation time that are included in Table 1. A comparison with the hydrodynamic theory of Tirado and Garcia de la Torre[32,33] (TG) for rigid rods, eqs 9–14, is also included in this table. Estimating the rod dimensions of the superhelical plasmid from the superhelix parameter for DNA, we find that the translational diffusion coefficient is in excellent agreement with the theories for rodlike particles in solution. The rotational relaxation time, how-

Table 1. Translational and Rotational Diffusion at Low Concentrations

conc (mg mL^{-1})	$D_0 \times 10^8$ (cm^2 s^{-1})	$\tau \equiv (6\Theta_0)^{-1}$ (μs)
0.062[a]	5.7 ± 0.1	61 ± 21
0.103[a]	5.6 ± 0.2	84 ± 26
Tirado[b]	5.6	254
Broersma[c]	4.9	275

[a] Averaged over different scattering angles. [b] Theoretical infinite dilution values calculated from the expected dimensions for an equivalent rod and eqs 9–14. [c] Theoretical infinite dilution values calculated from the expected dimensions and the eqs in ref 57 corresponding to eqs 12–14.

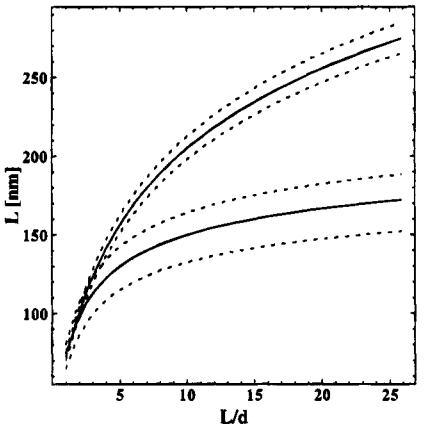

Figure 4. Determination of the axial ratio for the superhelical DNA assuming the rigid-rod model of Tirado and Garcia de la Torre (eqs 9–14).[32,33] The contour length L is calculated as a function of the axial ratio L/d for the measured translational (upper solid curve) and rotational (lower solid curve) diffusion coefficients. The intersection of these curves gives L/d and L that are consistent with both measurements. The dashed lines represent the curves calculated if the diffusion coefficient values at the extremes of the error bars are used. The L/d are between 1 and 3, values much lower than expected from calculations based on X-ray data for superhelical DNAs.

ever, is too fast by a factor of about 3. We can reverse this procedure and use the values of the translational and rotational diffusion coefficients to predict the dimensions of a hydrodynamically equivalent rod. To do this, we calculate the contour length L of the rod as a function of the axial ratio L/d using TG and our measured translational and rotational diffusion coefficients. For each of these diffusion coefficients we obtain a function. The two resulting functions are shown in Figure 4. The curves intersect at the point L_p/x_p which is consistent with both diffusion coefficients. We obtain hydrodynamic dimensions of length of 100 ± 10 nm and an axial ratio of 1–3 by this procedure.

It should also be mentioned that the measured rotational and translational relaxation times are in good agreement with values obtained by Langowski et al. for several plasmids with larger numbers of base pairs.[53,54] Figures 5 and 6 show the molecular weight dependence of the translational diffusion and rotational diffusion coefficients, respectively, for different plasmids. Our plasmid, which lies at the lower end of the molecular weight scale, fits in nicely with the curves presented by Langowski. A similar rotational relaxation time for the 2311 bp plasmid was also measured earlier by Lewis, Huang, and Pecora.[18] They found an apparent hydrodynamic radius at a scattering angle of 90° of 16 nm for the faster process which compares well with the 14 nm we obtain. The hydrodynamic radius of 38 nm, calculated from the translational diffusion coefficient of the plasmid, agrees also with the empirical relation between sedimentation constants and molecular

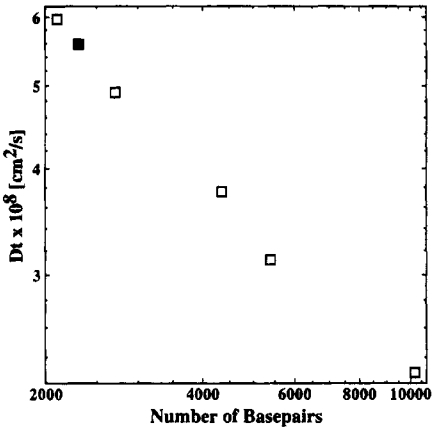

Figure 5. Molecular weight dependence of the translational diffusion coefficient. The open squares represent data taken from refs 53 and 54. The solid square represents the diffusion coefficient for the 2311 bp superhelical DNA.

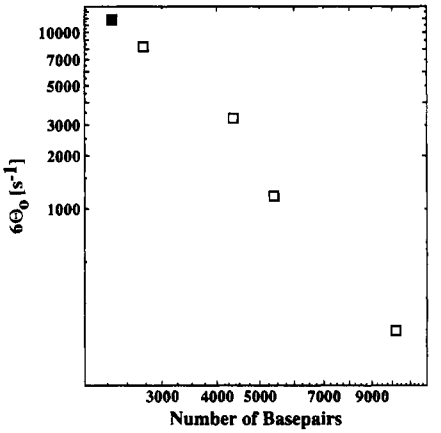

Figure 6. Molecular weight dependence of the rotational diffusion coefficient. The meaning of the symbols is the same as in Figure 5.

weights.[55] With the sedimentation constant and the Svedberg equation, we would calculate a radius of 40 nm.

4.3. Hydrodynamics of Simulated Rigid Shapes. There are several possible explanations for these results. First, the plasmid might not be rodlike. In fact electron micrographs from longer superhelical plasmids clearly show that the molecules are not rodlike. Instead one observes kinks and loops coming out of the long axis of the molecule.[18] To mimic such a structure, we used the procedure of Tirado and Garcia de la Torre (summarized above in eqs 3–8) to calculate hydrodynamic properties of rigid bodies. Rings of four touching beads were generated and then assembled in various irregular shapes (Figure 7). As a test of the procedure, a rigid rod was generated by stacking four-membered rings on top of each other. As can be seen from Table 2, the calculated translational and rotational diffusion coefficients of the test rod are close to the ones predicted by eqs 9–11. In fact, Tirado and Garcia de la Torre used the same procedure and extrapolated the bead size to zero (number of beads → ∞) to obtain the given equations.

It is evident from Table 2 that these irregular shapes produce rotational diffusion coefficients which are much closer to the experimental ones. However, this agreement can only be achieved by a simultaneous deviation of the calculated corresponding translational diffusion coefficient from the experimental value. This discrep-

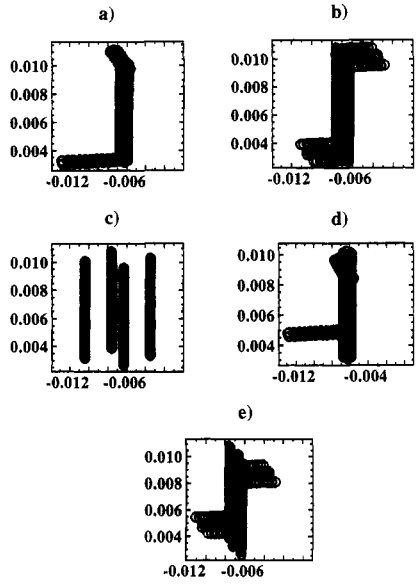

Figure 7. Generated shapes to simulate the hydrodynamics of superhelical DNA. All shapes are built from stacked four-membered rings consisting of touching beads. (The bead size in the figure is not the one actually used.) Shape c is a rigid rod. The others are generated from this shape by rotating parts of the rod and attaching them on the sides. For more details see the description in Table 2.

Table 2. Translational and Rotational Diffusion of Irregularly Shaped Objects

structure description[a]				hydrodynamics		
offset 1	offset 2	bn 1	bn 2	$D_0 \times 10^8$ (cm^2/s)	τ^b (μs)	$\tau_g{}^c$ (μs)
1/2	81/2	1	4	6.08	200	250
1/2	81/2	1	3	5.89	217	273
0	0	1	3	5.92	198	394
10	32	1	4	7.70	121	65
10	32	1	3	6.41	141	260
0	0	0	0	5.80	336	99

[a] The starting rod structure consists of 62 stacks of rings formed by four touching beads with a diameter of 1 nm. It is the last structure in Table 2 and is described by offset 1 = offset 2 = bn 1 = bn 2 = 0. The first ring is placed in the xy plane with coordinates 0,0,0 for the center of the ring. The z coordinates of the following stacks are then incremented by 1 (ranging therefore from 0 to 61). 10 stacks are now taken from this structure and rotated by 90° around the y or x axes, and the center of the lowest stack is then attached at a z coordinate which is given by offset 1 and is oriented along the line which is defined by (0,0,offset 1) and (x,y,offset 1). The x and y coordinates are taken from bead number bn 1 plus one bond length. Another 10 stacks are treated in the same way. Their coordinates are defined by offset 2 and bn 2. All resulting structures consist of a central rod formed by 42 stacks and two arms each of 10 stacks. The positions of the arms along the central rod are defined by offset 1 and offset 2. For each structure there exists a cis (bn 1 = 1, bn 2 = 4) and a trans configuration (bn 1 = 1, bn 2 = 3). The configurations described by bn 1 = 2 and bn 2 = 3 or bn 1 = 1 and bn 2 = 2 are all cis conformations and equivalent to bn 1 = 1 and bn 2 = 4. [b] Long axis orientation. [c] Calculated from the trace of the rotational diffusion tensor.

ancy has been observed by other authors who have studied superhelical DNAs with similar numbers of base pairs. It is possible that some internal mode of motion is contributing to the scattered light time correlation function, although our present data are insufficient to draw any further conclusions.

4.4. Evidence for Two Hydrodynamic Regimes. The clearest evidence for two different hydrodynamic regimes comes from a plot of $\log(D/D_0)$ versus $\log(cL^3)$ shown in Figure 8. D_0 was determined by extrapolating the five lowest concentrations to zero. The contour

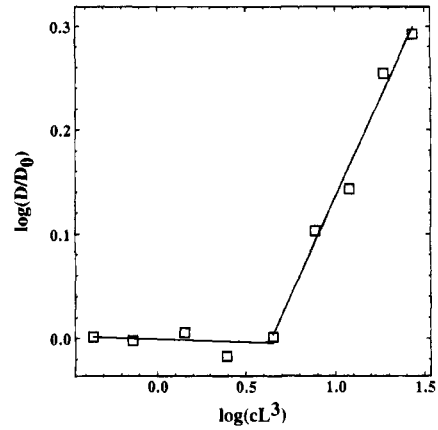

Figure 8. Concentration dependence of the mutual diffusion coefficient (log–log plot). The lowest concentration data point corresponds to 0.06 mg mL^{-1} and the highest to 3.8 mg mL^{-1}.

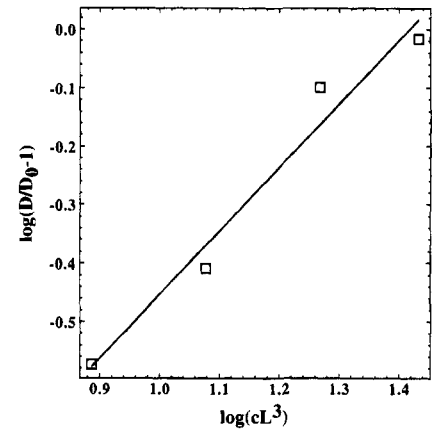

Figure 9. Concentration dependence of the mutual diffusion coefficient. Determination of the power law.

length L was assumed to be the value calculated from the rod model for superhelical DNA presented in section 2.4. A dramatic change in slope in the region $cL^3 = 3-5$ is observed. We take this region to locate the boundary between the virial and semidilute regimes. Moreover, in this boundary concentration region, the slow mode begins to appear in the measured correlation functions. From the slope of the straight line of the log–log plot in Figure 8, we determine a scaling exponent of 0.30 ± 0.01 for the concentration dependence of the mutual diffusion coefficient in the semidilute regime. This value of the exponent is much lower than experimentally found and also theoretically predicted from scaling theories for flexible polymers. The occurrence of the beginning of the semidilute regime at cL^3 from 3 to 5 is in reasonable accord with (although somewhat lower than) values found for other rodlike systems.[1]

4.5. Concentration Dependence of the Mutual Diffusion Coefficient. The scaling exponent of 0.30 for the concentration dependence determined in the previous section does not contradict the linear concentration dependence predicted by the DSO theory. The scaling approach stands on different physical grounds than DSO. In fact, the scaling approach is unphysical in the sense that extrapolated to zero concentration the diffusion coefficient becomes zero. The DSO theory, however, leads to D_0 for infinite dilution. In order to test the concentration dependence predicted by DSO (eq 22), a plot of log ($D/D_0 - 1$) versus log(cL^3) was made. Such a plot is shown in Figure 9 for the points in the semidilute regime. The exponent determined is practically 1, and the intercept of the D/D_0 versus cL^3 line is

Table 3. Concentration Dependence of Mutual Diffusion Coefficients

exponent semidilute	1.1 ± 0.1 (slope of line in Figure 9)
intercept semidilute	1.0 ± 0.1 (intercept in Figure 9)
k semidilute	0.058 ± 0.009
k_D semidilute[a]	273 ± 44 cm^3 g^{-1}
k_D dilute[a]	−130 ± 82 cm^3 g^{-1}
k_ϕ dilute[b]	−12 ± 8
k_ϕ semidilute[b]	26 ± 4
k_ϕ semidilute 236[c]	31 ± 2
k_ϕ semidilute PBLG[d]	10 ± 1
k_ϕ dilute PBLG[e]	−3 ± 3
k_ϕ dilute 2311[f]	225 ± 52

[a] $k_D = kN_AL^3/M$. [b] $k_\phi = k_DM/(N_AV_h)$. [c] This k_ϕ was determined for a 236 bp linear DNA by Goinga and Pecora.[11] The value of k_f here is different from that reported by Goinga and Pecora. The reason is that they used the volume of a sphere determined by the hydrodynamic radius r_h in order to compare their results with those for more flexible polymers. Here we use the volume of a rod. The advantage is that a possible flexibility of the molecule would result in a much higher value for k_ϕ calculated in this way. One can convert the Goinga and Pecora k_ϕ' into k_ϕ by $k_\phi = 3Ld^2k_\phi'/(16r_h^3)$. [d] This k_ϕ was obtained for PBLG by Tracy and Pecora in the semidilute regime.[24] The k_ϕ for this neutral polymer is at least a factor of 3 smaller than for charged molecules like DNA. [e] This k_ϕ was obtained for PBLG by Tracy and Pecora[24] in the dilute regime. [f] The 2311 bp linear DNA is a semiflexible molecule. Therefore, k_ϕ is much higher than for stiff molecules, if we assume the hydrodynamic volume can be calculated from the cylinder defined by the contour length L and the diameter d (see also footnote c).

also 1, as is required. The data for the concentration dependence of the mutual diffusion coefficients are summarized in Table 3. A linear concentration dependence of the mutual diffusion coefficient in the semidilute regime is thus consistent with the data for this system. This linear dependence is in agreement with the prediction of DSO theory for the concentration dependence of the cooperative diffusion coefficient for rigid uncharged rods. The slopes of the concentration dependences in the virial and semidilute regimes are in good agreement with measurements on other rodlike polymers as indicated by the k_ϕ given in Table 3. The slope in the semidilute regime for the superhelical plasmid DNA is larger by a factor of about 3 than for neutral polymers like PBLG but very similar to those for charged rods like short linear DNA. In order to compare the slope in the semidilute regime with that of the DSO prediction (Figure 10), assumptions about the concentration dependence of the self-diffusion coefficient must be made. Figure 10 is based on eq 4.12 of ref 9 for τ_2. There it is assumed that the self-diffusion coefficient is constant in the semidilute regime and the transverse diffusion is completely frozen. We discuss this point as well as alternate assumptions in more detail below.

4.6. Concentration Dependence of the Fast Relaxation Time. As discussed above, a fast relaxation mode is observed in addition to the translational mode. The amplitudes and relaxation frequencies of this mode can be followed from the dilute through the semidilute regimes. Subtracting the frequency of the translational mode from the frequency of this fast mode leads to a relaxation time that is independent of the scattering vector length. We shall call this time the "rotational relaxation time" of the molecule, although, as discussed above, in dilute solution it is not consistent with the rotational relaxation time of a rod with our calculated dimensions. The time is shown to be independent of the scattering vector length for two concentrations in the dilute regime (Figure 11). The mean

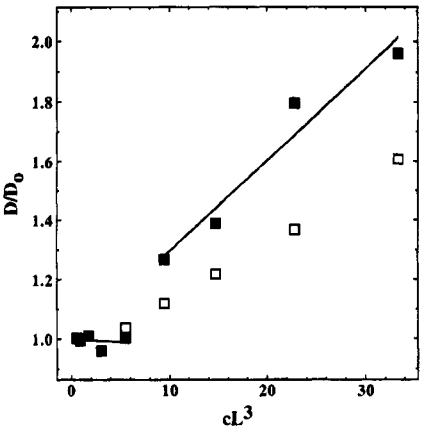

Figure 10. Concentration dependence of the mutual diffusion coefficient (solid squares). Comparison with the DSO theory (open squares).

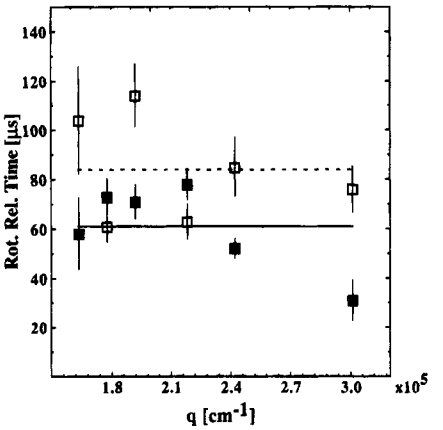

Figure 11. Apparent rotational relaxation times as a function of the scattering vector length. The different symbols indicate concentrations of 0.06 (solid squares) and 0.20 mg mL^{-1} (open squares).

relaxation time averaged over several scattering angles shows a slight concentration dependence, as may be seen in Figure 12. The relative amplitude of the fast mode to the translational mode is plotted in Figure 13. As required for the contribution of a rotational internal mode to the correlation function, the relative amplitude increases with increasing scattering vector length. Especially at higher concentrations, the uncertainty in the relaxation times is rather high due to the low amplitude of this fast process compared to the amplitude of the slow mode and the pure translational mode. Thus, the data are not sufficiently precise to conclude whether or not the rotational relaxation time shows a linear concentration dependence or even if it levels off at higher concentrations. The rotational relaxation time does appear to level off if one focuses on the mean values only. A quadratic concentration dependence as predicted by DE (eq 21) does not appear to be consistent with the data.

4.7. The Slow Mode. At the highest concentration of DNA measured, the slow mode is by far the dominant mode. For this concentration, the slow mode is clearly diffusive; it exhibits a quadratic dependence on scattering vector length, as shown in the top part of Figure 14. A further characteristic of this mode is that its relative contribution to the correlation function decreases with increasing scattering vector length. This is shown in the bottom part of Figure 14. Both properties are characteristic of the diffusion of a particle that is larger than the inverse length of the scattering vector.

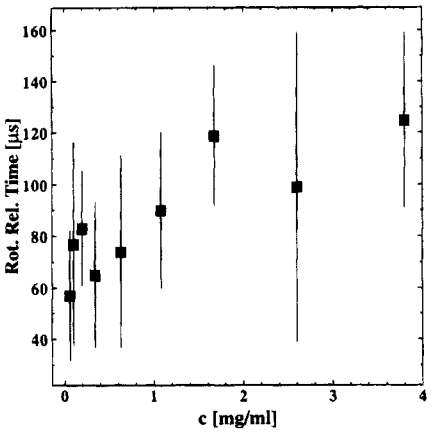

Figure 12. Concentration dependence of the apparent rotational relaxation times. Each displayed time is a weighted average of measurements at different scattering angles. The relative amplitudes of the mode were taken as weighting factors. In some rare cases a mode was excluded from the average when it was clear from its amplitude that other modes, in particular the translational mode, were mixed in. In other rare cases, an additional fast mode with a very small amplitude together with an unusual slow apparent rotational relaxation mode was observed. Under these circumstances the two fast modes were first averaged. In general, these difficulties occurred for the measurements at higher concentrations where the slow mode was also present.

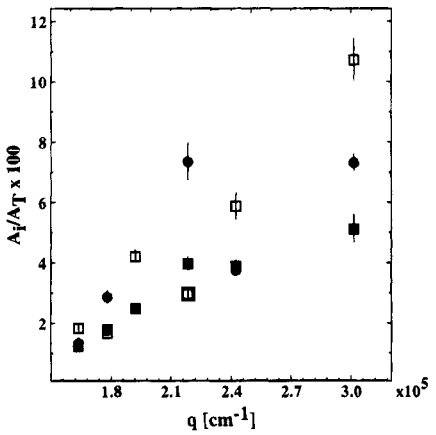

Figure 13. Relative contribution of the fast mode A_f/A_T as a function of the scattering vector length q. The A_T is the total amplitude of the first-order correlation function ($g_1(q,t)$), which is the same as the area under the frequency distribution. The symbols represent polymer concentrations of 0.06 (solid squares), 0.10 (solid circles), and 0.20 (open squares) mg mL^{-1}.

The largest q data points in Figure 14 exhibit larger uncertainties since there appeared to be some merging of the modes at these high scattering angles. A comparison of the relative intensity of the slow mode to that of the fast mode (calculated at q's corresponding to a 90° scattering angle) and the ratio of the fast decay time to the slow mode decay time to the predictions of DSO is given in Table 4. The relative decay times are in good agreement with the predictions of DSO. The concentration dependence of the slow mode intensity (column 4 of Table 4), however, rules out an identification of this mode with the slow mode predicted by DSO for hard uncharged rods. For DSO a decreasing amplitude with increasing concentration is predicted. We observe an increase of the amplitude of this mode with increasing concentration, as shown in Figure 15.

V. Discussion and Conclusions

5.1. Single Particle Hydrodynamic Properties. The value of the fast relaxation time in dilute solution,

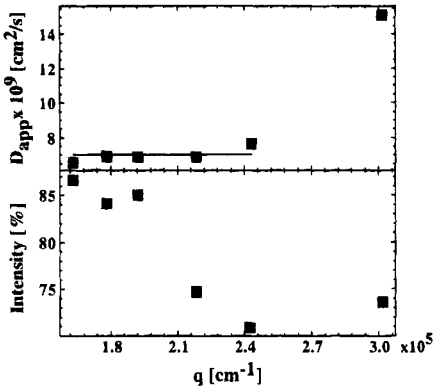

Figure 14. Top: Scattering vector length (q) dependence of the diffusion coefficient of the slow mode. Bottom: Scattering vector length (q) dependence of the contribution of the slow mode to the correlation function. The data are for the highest concentration solution studied, 3.8 mg mL^{-1}.

Table 4. Predictions of the Spinodal Decomposition DSO Theory[a]

cL^3	c/c^*	A_s	A_s(meas)	τ_c/τ_s	τ_c/τ_s(meas)
33.3	0.244	22	84	0.125	0.08 ± 0.02
22.8	0.168	30	42	0.147	0.13 ± 0.04
14.7	0.108	39	44	0.162	0.17 ± 0.07
9.5	0.069	47	35	0.167	0.18
5.5	0.040	54	0	0.166	0.24

[a] The slow mode is indexed with s, the fast one with c (see eqs 27–29). The c^* defines the onset of an extraordinary phase and is given by $c^* = 16/(\pi dL^2)$. It should not be confused with the concentration where entanglements become important. Note that the ratio of relaxation times is in fairly good agreement with the predictions of DSO and that both relaxation times are well separated in the concentration range studied. But the amplitude of the slow mode shows just the opposite behavior with concentration than predicted by DSO.

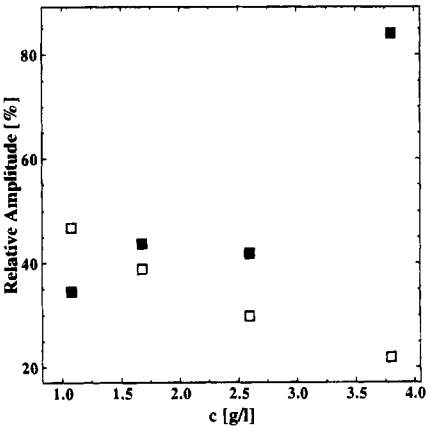

Figure 15. Comparison of the relative contribution of the slow mode (solid squares) with the prediction of the DSO theory (open squares).

interpreted as a rotational relaxation time around an axis perpendicular to the long axes of a cylinder, would lead us to the conclusion that the axial ratio of the 2311 bp plasmid DNA is much lower than expected from structural helix data. First we estimate the effect translational–rotational coupling might have on the measured rotational relaxation time. The calculation is straightforward using eq 17 of ref 29 for the polarized scattering case. For a 230 nm long rod with a diameter of 14 nm, the apparent translational diffusion coefficient would be 5.9×10^{-8} cm^2 s^{-1} and the rotational relaxation time 234 μs. The contribution of the rotational relaxation time to the decay of the correlation function at a scattering angle of 90° would be 4.3% of the total

amplitude. The contribution of the rotational relaxation mode is smaller if translational–rotational coupling is taken into account. Given the experimental error, the contributions of this mode displayed in Figure 13 are consistent with either theory. The corrections to the relaxation times due to coupling are relatively small, so that the discrepancies cannot be explained by the effects of translational–rotational coupling.

Modeling the plasmid as an irregular rigid shape that is based on the superhelix structure from X-ray data does not reproduce the hydrodynamic properties of the plasmid either. Two additional possibilities exist which might lead to a faster experimental "internal" relaxation time. First, the plasmid might not be as stiff as expected. Then PCS would likely monitor the relaxation time of a semistiff rod. Wormlike chain theories would be more appropriate to calculate these times and relate them to the structure and stiffness of the chain. Yoshizaki and Yamakawa[56] have used the discrete helical wormlike chain model to relate the ratio of slowest relaxation time τ_w of the chain and the rotational relaxation time (τ_{rod}) of a rod to the number of Kuhn segments $N_k = L/2a$, where a is the persistence length:

$$\tau_w/\tau_{rod} = \frac{[N_k + 0.5(\exp(-2N_k) - 1)]^{3/2}}{N_k^3}[1 + 0.539526 \ln(1 + N_k)] \quad (38)$$

$\tau_{rod} = 1/(6\Theta)$ has to be calculated according to the Broersma formula,[57] which is similar to eq 11 with different end-effect corrections (eq 14). A persistence length could be derived for the plasmid by substituting measured τ_w and τ_{rod} for a cylinder of length of 230 nm and diameter of 14 nm into eq 38.

In an alternative approach, the Monte Carlo results of Hagerman and Zimm[58] on an ensemble of wormlike coil configurations could be used to relate the rotational diffusion constant of a wormlike chain to that for a rod (calculated using Broersma's formula). Again, a persistence length can be obtained from this comparison.

Using either approach leads to persistence lengths for the plasmid that are unrealistically small. For the Hagermann–Zimm approach we obtain 45 nm, and eq 38 leads to 46 nm. It should also be mentioned that 45 nm is near the upper limit of validity stated for the Hagerman–Zimm approach ($L/a < 5$). Thus, the factor of 3 faster than expected internal relaxation time cannot be explained by the wormlike chain theories unless an unrealistic assumption about the rigidity of the molecule is made.

A possible explanation for this descrepancy could, however, be that the plasmid exhibits more flexibility than expected. The consequent deviations from rodlike shape could be large enough that rotation around the elongated axis of the wormlike chain contributes to the light scattering time correlation function. The procedure of Tirado and Garcia de la Torre for calculating hydrodynamic properties of rigid macromolecules can be used to calculate the trace of the rotational diffusion tensor. The rotational relaxation time derived from the trace may be used as a rough estimate of this effect. Table 2 shows that the relaxation time derived in this way from the presumed dimensions and stiffness of the plasmid is consistent with the experimental result.

5.2. Mutual Diffusion in the Virial Regime. The concentration dependence of the mutual diffusion coefficient in the virial regime is an additional indicator of the underlying shape of the plasmid DNA. Information on the shape of the molecule directly enters into the calculation of the osmotic second virial coefficient and the friction term as indicated in eqs 17–20. Substituting the parameters for the plasmid DNA (assuming the rod dimensions discussed in section 2.4) into these equations, we obtain values of A_2, k_f, and k_D (see Table 3). Although the experimental k_D exhibits a rather large uncertainty, the theoretical prediction is clearly outside the range of the experimental value. The discrepancy, however, can be rationalized by taking the charges on the rod into account. For charged rods the diameter entering in eq 18 to calculate A_2 might be interpreted as an effective interaction diameter d_e and not the geometric diameter d of the molecule. The d_e should be a function of the ionic strength and, in principle, could be calculated from Stigter's theory.[59,60] We note that the term containing A_2 exhibits a much stronger dependence on d than k_f and should therefore dominate. We therefore expect A_2 to be approximately a factor of 2.5 larger than that given by eqs 18 and 19. This leads to an effective diameter $d_e = 2.5d$. Determination of A_2 from total intensity measurements on a short linear DNA fragment supports such an interpretation of the diameter in eq 18.[11,21] The same argument might also hold in the semidilute regime as we discuss below.

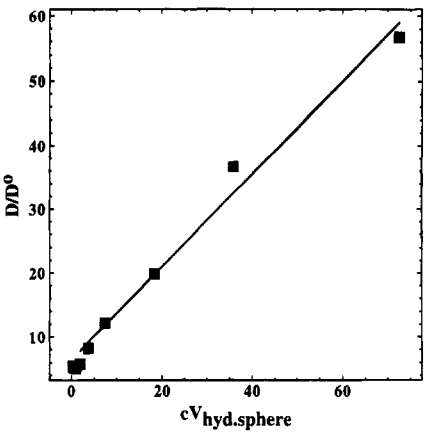

Figure 16. Concentration dependence of the mutual diffusion coefficient for poly(adenylic acid). The data are taken from Figure 5 of Mathiez et al.[61] L^3 is replaced by the volume of an equivalent hydrodynamic sphere for this flexible molecule. The radius of the sphere was calculated from the reported D_0.

5.3. Mutual Diffusion in the Semidilute Regime. An important result of our study is the clearly different slopes for the concentration dependence of the mutual diffusion coefficient in the semidilute and virial regimes. This has often been overlooked in previous studies due to a limited number of experimental points in either regime. Recently, however, in studies of solutions of poly(γ-benzyl α,L-glutamate) (PBLG) in dimethylformamide, the two regimes were also observed.[22,24] As in previous studies of rodlike polymers, a linear concentration dependence of the mutual diffusion coefficient in the semidilute regime is found. This linear behavior is, however, in itself, a rather weak test of the validity of the DSO theory, as well as weak proof of rodlike molecular shape. Since functions of the scaling form $D_m \sim D_0 c^\epsilon$ and of linear concentration dependence $D_m \sim D_0(1 + kc)$ do not exclude each other, the data of Mathiez et al.[61] on a flexible single-stranded poly(adenylic acid) were reanalyzed. Instead of a fit to the scaling equation, as was done by the authors, a linear fit was performed. Figure 16 indicates that it is a good

fit to their data. It is possible that the linear concentration dependence of D_m in the semidilute regime is universal, appearing no matter what the conformation of the molecule. With the slope of the concentration dependence of D_m and the overlap concentration c^* itself, however, we have two parameters to perform strong tests on theory and the shape of our molecule.

Unfortunately, as has already been discussed in section 4.5, additional assumptions about the concentration dependence of the self-diffusion coefficient must be made in order to compare the experimental slope with DSO theory. The original DE assumptions were made to calculate the theoretical points in Figure 10. Alternatively, it could be assumed that the self-diffusion coefficient is constant and equals D_0 in the infinite dilution limit, as has, for instance, been done by Goinga and Pecora.[11] In such a case, the slope in the DSO theory would be a factor of 2 higher than the experimental results, in agreement with Goinga and Pecora. In both cases, it was assumed that the geometric diameter is the appropriate one to use. This assumption might not be valid for charged rods, as has already been discussed elsewhere.[11]

There is strong evidence from HGR[12] and BD simulations[13,14] that the self-diffusion coefficient depends also on concentration. The HGS data from Wang et al. for a 150 bp DNA fragment can be used to make a rough comparison.[12] Data from Figure 10 of Wang et al.[12] were fit to a straight line to obtain the slope k_s of the concentration dependence of D_s. If we further assume that

$$k_\phi = k_s M/N_A V_h \tag{39}$$

is the same for the linear and superhelical DNAs, the slope of the theoretical DSO line (eq 22) in Figure 10 can be corrected (dropping terms quadratic in c, taking the $q \to 0$ limit). The M, N_A, and V_h in eq 39 are the molecular mass, Avogadro's constant, and the hydrodynamic volume, respectively. After these corrections are performed, the slopes of the experimental line and the DSO theory line are found to differ by only a factor of 1.3. This factor might be explained by the charges on the plasmid DNA. As has already been discussed for the virial regime, an effective interaction diameter d_e according to the theory of Stigter might be more appropriate to use in eq 18 to calculate the second osmotic virial coefficient. Stigter gives the relation

$$d_e = d \exp(g/2) \tag{40}$$

where g/Φ_0^2 is tabulated in ref 60 for a number of Φ_0 and κd. The quantity κ is the inverse of the Debye screening length and Φ_0 is a reduced surface charge. The latter quantity is not known for superhelical DNA, but it should be higher than that for linear DNA due to the folidng of the molecule. To obtain an estimate of the effect, we used the highest value tabulated for Φ_0 at $\kappa d = 0.2$ and assumed equal conductivities for counterions and co-ions (for NaCl solutions this is not correct). For such high surface charges the effect should be quite substantial as the calculated d_e of 16.5 nm, an increase of 23%, indicates.

In several publications on rodlike systems, it was noted that semidilute behavior (as indicated by a break in the slope of the translational diffusion coefficient or a strong slowing down of the rotational diffusion coefficient) starts at concentrations approximately a factor of 5−15 higher than the overlap concentration ($cL^3 =$ 1). Our value, $c^*L^3 \approx 5$, is near the lower end of this range. This is an indication that the derived length for the plasmid DNA is likely not much lower than that used here. The value of k_ϕ for the plasmid, which we suppose to be universal for different DNAs, gives us some confidence that the superhelical DNA is at least approximately rodlike.

5.4. Concentration Dependence of the Rotational Diffusion Coefficient. Within the rather large errors, there is no indication of two different concentration regimes for the rotational diffusion coefficient. The apparent slowing down of the rotational diffusion is qualitatively in agreement with theoretical considerations, especially the Fixman relaxation model. The scatter in the data is too large for a more quantitative comparison between theory and experiment.

5.5. The Slow Mode. The nature of the slow mode in semidilute solutions in general, as well as in particular for DNA solutions, has long been the subject of controversy.[25,62-67] Different explanations for the origin of this mode have been given. They have been recently summarized by Goinga and Pecora,[11] Sedlak,[66] and Reed.[67] There is a major difference between our data and previous data on short duplex linear DNA fragments. Since the superhelical plasmid DNA is a factor of about 3 longer than a 236 bp linear DNA, we were able to perform measurements further into the semidilute regime. For the highest concentration, the slow mode became the dominant relaxation process. We also covered the whole decay of the DLS correlation functions by splicing correlation functions with different time ranges.

Focusing again on the spinodal decomposition part of the DSO theory, we conclude that the experimentally observed slow mode cannot be identified with that predicted by this theory. The increasing contribution of this mode to the total relaxation with increasing polymer concentration is opposite to the prediction of the theory. The dependences of the mode amplitude and frequency on concentration are different from those previously reported for linear DNA. A possible reason for this discrepancy could lie in the limited time range of the previous measurements and the low amplitude of the slow mode. Our experiments, however, demonstrate again a q^2 dependence of the decay rate of this mode as well as the decrease of its amplitude with increasing scattering vector length. These facts strongly favor "aggregates" as the most plausible explanation for the origin of the slow mode. Increasing the concentration leads to growth of the aggregates, with a corresponding slowing down of the relaxation frequency and an increase in amplitude. Why these aggregates are not detected in self-diffusion measurements with the holographic grating relaxation technique is currently not understood.[12]

Acknowledgment. This work was supported by National Science Foundation Grant CHE-9119676 to R.P. and by the NSF−MRL program through the Center for Materials Research at Stanford University. J.S. is greatly indebted to the Deutsche Forschungsgemeinschaft (DFG) for their extended financial support (Grant Se533/2) of his stay at Stanford University. We also thank Prof. Garcia de la Torre for providing us with a version of his FORTRAN subroutine TRV to calculate hydrodynamic properties of an assembly of beads. R.P. thanks Professor E. W. Fischer for his hospitality at the Max-Planck-Institute for Polymer Research, Mainz, Germany, where part of this manuscript was written.

References and Notes

(1) Tracy, M. A.; Pecora, R. *Annu. Rev. Phys. Chem.* **1992**, *43*, 525.
(2) Doi, M.; Edwards, S. F. *J. Chem. Soc., Faraday Trans. 2* **1978**, *74*, 560.
(3) Doi, M.; Edwards, S. F. *The Theory of Polymer Dynamics*; Clarendon Press: Oxford, U.K., 1986.
(4) Brochard, F.; de Gennes, P.-G. *Macromolecules* **1977**, *10*, 1157.
(5) de Gennes, P.-G. *Scaling Concepts in Polymer Physics*; Cornell University Press: Ithaca, NY, 1979.
(6) Keep, G. T.; Pecora, R. *Macromolecules* **1988**, *21*, 817.
(7) Shimada, T.; Doi, M.; Okano, K. *J. Chem. Phys.* **1988**, *88*, 2815.
(8) Doi, M.; Shimada, T.; Okano, K. *J. Chem. Phys.* **1988**, *88*, 4070.
(9) Shimada, T.; Doi, M.; Okano, K. *J. Chem. Phys.* **1988**, *88*, 7181.
(10) Russo, P. S.; Karasz, F. E.; Langley, K. H. *J. Chem. Phys.* **1984**, *80*, 5312.
(11) Goinga, H. T.; Pecora, R. *Macromolecules* **1991**, *24*, 6128.
(12) Wang, L.; Garner, M. M.; Yu, H. *Macromolecules* **1991**, *24*, 2368.
(13) Bitsanis, I.; Davis, H. T.; Tirell, M. *Macromolecules* **1988**, *21*, 2824.
(14) Bitsanis, I.; Davis, H. T.; Tirell, M. *Macromolecules* **1990**, *23*, 1157.
(15) Fixman, M. *Phys. Rev. Lett.* **1985**, *54*, 337; *55*, 2429.
(16) Strzelecka, T. E.; Rill, R. L. *Macromolecules* **1991**, *24*, 5124.
(17) Russo, P. S.; Miller, W. G. *Macromolecules* **1983**, *16*, 1690.
(18) Lewis, R. J.; Huang, J. H.; Pecora, R. *Macromolecules* **1985**, *18*, 944.
(19) Lewis, R. J.; Pecora, R.; Eden, D. *Macromolecules* **1986**, *19*, 134.
(20) Lewis, R. J.; Pecora, R.; Eden, D. *Macromolecules* **1987**, *20*, 2579.
(21) Nicolai, T.; Mandel, M. *Macromolecules* **1989**, *22*, 2348.
(22) DeLong, L. M.; Russo, P. S. *Macromolecules* **1991**, *24*, 6139.
(23) Graf, C.; Deggelmann, M.; Hagenbüchle, M.; Kramer, H.; Krause, R.; Martin, C.; Weber, R. *J. Chem. Phys.* **1991**, *95*, 6284.
(24) Tracy, M. A.; Pecora, R. *Macromolecules* **1992**, *25*, 337.
(25) Ferrari, M. E.; Bloomfield, V. A. *Macromolecules* **1992**, *25*, 5266.
(26) Berne, B. J.; Pecora, R. *Dynamic Light Scattering*; Krieger Publishing Co.: Malabar, FL, 1990.
(27) Pecora, R. *J. Chem. Phys.* **1968**, *48*, 4126.
(28) Maeda, H.; Saito, N. *Polym. J.* **1973**, *4*, 309.
(29) Rallison, J. M.; Leal, L. G. *J. Chem. Phys.* **1981**, *74*, 4819.
(30) Aragon, S. R.; Pecora, R. *J. Chem. Phys.* **1985**, *82*, 5346.
(31) Perrin, F. *J. Phys. Radium* **1934**, *5*, 497; **1936**, *7*, 1.
(32) Tirado, M. M.; Garcia de la Torre, J. *J. Chem. Phys.* **1980**, *73*, 1986.
(33) Tirado, M. M.; Garcia de la Torre, J. *J. Chem. Phys.* **1984**, *81*, 2047.
(34) Kirkwood, J. G. *J. Chem. Phys.* **1948**, *16*, 565.
(35) Garcia de la Torre, J.; Jimenez, A.; Freire, J. J. *Macromolecules* **1982**, *15*, 148.
(36) Harvey, S. C.; Mellado, P.; Garcia de la Torre, J. *J. Chem. Phys.* **1983**, *78*, 2081.
(37) Rotne, J.; Prager, S. *J. Chem. Phys.* **1969**, *50*, 4381.
(38) Yamakawa, H. *J. Chem. Phys.* **1970**, *53*, 436.
(39) Eimer, W.; Williamson, J. R.; Boxer, S. G.; Pecora, R. *Biochemistry* **1990**, *29*, 799. Eimer, W.; Pecora, R. *J. Chem. Phys.* **1991**, *94*, 2324.
(40) Han, C. C.; Akcasu, A. Z. *Polymer* **1981**, *22*, 1165.
(41) Yamakawa, H. *Modern Theory of Polymer Solutions*; Harper and Row: New York, 1971.
(42) Peterson, J. M. *J. Chem. Phys.* **1964**, *40*, 2680.
(43) Itou, S.; Nishioka, N.; Norisuye, T.; Teramoto, A. *Macromolecules* **1981**, *14*, 904.
(44) Benham, C. J.; Brady, G. W.; Fein, D. B. *Biophys. J.* **1980**, *29*, 351.
(45) Bauer, W.; Vinograd, J. *J. Mol. Biol.* **1970**, *47*, 419.
(46) Brady, G. W.; Foos, D.; Benham, C. J. *Biopolymers* **1984**, *23*, 2963.
(47) Newman, J. *Biopolymers* **1984**, *23*, 1113.
(48) Marko, M. A.; Chipperfield, R.; Birnboim, H. C. *Anal. Biochem.* **1982**, *121*, 382.
(49) Lee, S.; Rasheed, S. *BioTechniques* **1990**, *9*, 676.
(50) Seils, J.; Pecora, R. *Macromolecules* **1992**, *25*, 354.
(51) Provencher, S. W. *Comput. Phys. Commun.* **1982**, *27*, 213.
(52) Provencher, S. W. *Comput. Phys. Commun.* **1982**, *27*, 229.
(53) Langowski, J. *Biophys. Chem.* **1987**, *27*, 263.
(54) Langowski, J.; Giesen, U. *Biophys. Chem.* **1989**, *34*, 9.
(55) Hudson, B.; Vinograd, J. *Nature* **1969**, *221*, 332.
(56) Yoshizaki, T.; Yamakawa, H. *J. Chem. Phys.* **1984**, *81*, 982.
(57) Broersma, S. *J. Chem. Phys.* **1960**, *32*, 1626; **1981**, *74*, 6989.
(58) Hagerman, P. J.; Zimm, B. H. *Biopolymers* **1981**, *20*, 1481.
(59) Stigter, D. *Macromolecules* **1985**, *18*, 1619.
(60) Stigter, D. *J. Phys. Chem.* **1982**, *86*, 3553.
(61) Mathiez, P.; Mouttet, C.; Weisbuch, G. *Biopolymers* **1981**, *20*, 2381.
(62) Lin, S.; Lee, W.; Schurr, J. M. *Biopolymers* **1978**, *17*, 1041.
(63) Schmitz, K. S.; Lu, M. *Biopolymers* **1984**, *23*, 797.
(64) Schmitz, K. S.; Lu, M.; Singh, N.; Ramsay, D. J. *Biopolymers* **1984**, *23*, 1637.
(65) Fried, M. G.; Bloomfield, V. A. *Biopolymers* **1984**, *23*, 2141.
(66) Sedlak, M. *Macromolecules* **1993**, *26*, 58.
(67) Reed, W. F. *Macromolecules* **1994**, *27*, 873.

MA941075O